doi.org/10.52568/001809/JCSP/47.06.2025

Sensing Properties of Au-Doped Stable Black Arsenic Phosphorus Monolayer for Small Gas Molecules

[1]Liujie Yang, [1]Xiaolei Li*, [2]Tengfei Wang, [1]Tiantian Xu, [1]Jiahao Yang

[1]Henan Polytechnic University, School of Materials Science and Engineering, Henan Key Laboratory of Materials for Deep Earth Engineering, Jiaozuo 454003, People's Republic of China.

[2]Key Laboratory of Soft Chemistry and Functional Materials of MOE, School of Chemistry and Chemical Engineering, Nanjing University of Science and Technology, Nanjing 210094, People's Republic of China.

Lixl@hpu.edu.cn*

(Received on 15th January 2025, accepted in revised form 5th May 2025)

Summary: This study first used phonon dispersion curves to validate the structural stability of the pristine α-phase black arsenic phosphorus (AsP) monolayer, and then combined molecular dynamics simulations to assess its structural stability under 300°C conditions, confirming its good stability. The stability of the Au-doped AsP monolayer(Au-AsP) was also assessed through simulations following doping. Once the material's stability was confirmed, the research explored modifications in the material's geometric structure, adsorption energies, charge transfer, orbital interactions in the electronic density of states (DOS) profile, and electronic band structure characteristics, after gas adsorption. The findings revealed that CO, NO_2, and NO molecules undergo chemical adsorption on the Au-AsP monolayer surface. During gas adsorption, notable characteristics such as rapid response and recovery times, significant charge transfer processes, as well as considerable alterations in conductivity and the work function of the material were observed. This study, for the first time, outlines a detailed gas-sensing mechanism for black arsenic phosphorus when exposed to small gas molecules, emphasizing its potential for sensing applications.

Keywords: DFT; black arsenic phosphorus; Gas sensing; Adsorption; Doped.

Introduction

Introduction

The rapid growth of heavy industries, the chemical sector, and the energy industry has led to a significant increase in emissions of industrial waste gases [1]. These emissions contain a variety of harmful substances, with carbon monoxide (CO), nitrogen monoxide (NO), and nitrogen dioxide (NO_2) being the most common and dangerous pollutants [2]. These gases not only contribute to air pollution but also present serious health hazards, with prolonged exposure potentially resulting in respiratory illnesses [3]. Similarly, the contamination of water bodies by pollutants such as chloramphenicol antibiotics and their derivatives, which pose significant environmental and public health risks, has raised similar concerns[4]. The presence of these harmful substances in industrial emissions and aqueous environments jeopardizes both air and water quality, contributing to a broader spectrum of environmental pollution. As such, the presence of these harmful gases and contaminants in industrial emissions and water sources poses a significant risk to both ecosystems and public health[5, 6]. Real-time detection and monitoring of these gases are crucial for implementing prompt actions to mitigate pollutant release and enhance the effectiveness of environmental management [7-9]. Consequently, the development of efficient and sensitive detection sensors has become a key focus of ongoing research in the rapidly evolving field of sensor technology[10-13].

Over the last ten years, nanomaterials have attracted considerable attention due to their broad application prospects, especially in the field of gas sensors[14-16].Nanoparticles of oxides, such as zinc oxide, are often used in the field of gas sensors due to their high surface area[17, 18]. However, their relatively poor sensitivity limits their application in high-performance gas sensors[19]. As a result, researchers have gradually shifted their focus towards two-dimensional materials, particularly monolayer two-dimensional materials. Among these, graphene, a unique material composed of a single atomically thin layer of carbon atoms arranged in a two-dimensional honeycomb lattice, initially gained widespread interest

*To whom all correspondence should be addressed.

due to its exceptional electrical, thermal, and mechanical properties [20]. At the same time, stanene has also demonstrated great potential in gas sensor applications due to its unique structure and excellent electronic properties[21, 22].However, the lack of a natural band gap limits their effectiveness in gas sensor applications [23]. As a result, researchers have been exploring alternative 2D materials for gas sensing. One promising material is phosphorene (α phase), which has emerged as a key focus in 2D semiconductor research because of its suitable band gap, excellent electronic properties, and remarkably high carrier mobility, making it highly suitable for advanced electronic applications and versatile sensing capabilities [24]. The unique wrinkled structure of phosphorene enhances gas molecule adsorption, leading to high sensitivity in gas sensing applications. Despite its promise, phosphorene still faces challenges related to environmental stability and controllability [25]. To overcome these issues, researchers have introduced arsenic (As) through alloying to enhance phosphorene's structural stability. This approach has led to the development of black arsenic phosphide, synthesized using efficient gas-phase transport methods, which has opened up new possibilities for laboratory research [26]. Compared to phosphorene, two-dimensional black arsenic phosphide exhibits a distinctive wrinkled structure that offers a larger surface area, enhancing carrier mobility up to 14,000 cm^2 V^{-1} s^{-1}, and featuring an appropriate direct band gap [27, 28]. Additionally, its adjustable chemical composition allows for the tuning of key physical properties, such as electronic and optical characteristics, further enhancing its potential in gas sensing research [29-31]. These properties make black arsenic phosphide ideal for investigating the gas sensing performance of AsP monolayer materials with various gas molecules.

Previous studies on the gas sensing properties of AsP monolayers have largely focused on structures with only As-P bonds [32, 33]. Although the high symmetry of this structure and the enhanced carrier mobility along the armchair direction are advantageous for research design, the AsP monolayer exhibits different structures with similar yet distinct properties. To address the diverse environmental conditions required for gas sensors and the demand for highly stable materials, further investigation into other structures is necessary. The AsP monolayer consists of a stoichiometric mix of arsenic and phosphorus (As:P = 1:1), resulting in three distinct allotropes. Among these allotropes, one exhibits zigzag bonds with alternating atomic pairs, such as P-As, P-P, and As-As. In the armchair direction, the dihedral angles between P-As-As and As-P-P are 99.9° and 103.2°, respectively, which counteract the impact of the longer P-As bonds. Additionally, the length of the As-P bond is 2.38 Å, which exceeds the P-P bond length in phosphorene by 0.16 Å.The P-As-P bond angle of 95.0°, together with the bond length, plays a crucial role in the structure, resembles the structure found in pure phosphorene, perhaps making this configuration the most stable among the three allotropes [34]. This study seeks to comprehensively investigate the fundamental adsorption characteristics and critical interaction properties of the stable α-phase AsP structure to ensure the consistent and reliable operation of gas sensors based on AsP materials in various environmental conditions.During the experimental design process, an analysis of existing research on the gas sensing performance of various two-dimensional materials revealed that many pristine 2D monolayers exhibit relatively weak adsorption properties for certain gases [35]. To address this limitation, researchers have employed techniques such as atomic doping to enhance the adsorption properties of these materials, thereby improving their gas sensing performance [36, 37]. Ma *et al* [38] . investigated the effects of Au, Pt, Pd, and Ni doping on CO and NO adsorption by molybdenum disulfide (MoS_2), concluding that doping markedly increases MoS_2's sensitivity compared to its undoped form. Li *et al* [39] .analyzed how aluminum and palladium doping affects H_2S adsorption by antimonide phosphorus (SbP), finding that doping significantly enhances SbP's sensitivity to gas molecules. Prasongkita *et al*. [40] examined the impact of doping on NO, CO, NH_3, and NO_2 adsorption by phosphorene, and demonstrated that doping considerably enhances phosphorene's sensitivity to these gases compared to the undoped form. Lin *et al* [41] studied the effects of Au-doped tin diselenide ($SnSe_2$) on CO, NO, and H_2O adsorption, showing that doping improves the interactions between gas molecules and the substrate surface. Wang *et al* [42] investigated the adsorption of gas molecules on a monolayer AsP surface with only As-P bonds using density functional theory (DFT) calculations, revealing that Au and Pt doping significantly enhances the sensitivity of the surface to NO and NO_2 molecules. Despite these recent developments, the intricate adsorption behavior and unique electronic properties of the CO, NO_2, and NO molecules on the most stable Au-doped α-phase AsP structures are still not fully understood. Thus, this study calculates the precise adsorption energy and significant charge transfer to effectively identify the optimal configurations for these gas molecules. This work uses first-principles

calculations to comprehensively investigate the detailed adsorption behavior and the changes in electronic properties of toxic gases, including CO, NO_2, and NO, on the most stable Au-doped α-phase AsP structure. It includes charge density difference (CDD), total density of states (TDOS), and projected density of states (PDOS). The proposed hypothesis offers a viable method for creating efficient black arsenic-phosphorus sensors capable of detecting toxic gases with high sensitivity.

Computational details

First-principles calculations based on the DFT were performed using the Vienna Ab-initio Simulation Package (VASP) [43]. This study employed the plane-wave basis set and the Perdew-Burke-Ernzerhof (PBE) functional within the generalized gradient approximation (GGA), due to its proven accuracy in producing the ground state structure of the adsorption system [44-46]. In the VASP calculations, GGA and DFT methods were used, but these methods have certain limitations in describing van der Waals (vdW) interactions. Specifically, GGA and traditional DFT methods fail to adequately consider weak interactions, such as van der Waals forces, which may lead to inaccurate results, especially when describing weak interactions like intermolecular or surface adsorption. Therefore, to address this limitation, the Grimme DFT-D3 method was employed in this study to correct the vdW interactions [47, 48]. For geometric optimization, we used the Conjugate Gradient method. Structural relaxation and total energy convergence were successfully achieved when the calculated forces on each individual atom were consistently below 0.01 eV/Å, and the energy difference between subsequent consecutive steps was significantly smaller than 10^{-5} eV.

In the calculations presented in this paper, a 3 × 4 × 1 supercell was used as the simulation cell. The doping concentration of Au atoms was 4.16%. A specific plane wave cutoff energy of 400 eV was employed, along with a k-point mesh chosen after multiple tests of 3 × 3 × 1. The detailed density of states (DOS) was meticulously calculated using a fine 10 × 10 × 1 k-point mesh. A sufficiently thick 20 Å vacuum layer was applied to effectively prevent any unwanted interactions between the periodic structures [49]. The molecular dynamics (MD) simulation was conducted on a 5 × 5 × 1 supercell of both pristine and doped AsP monolayers. The simulation employed a canonical ensemble with the Nose-Hoover thermostat at a temperature of 300 K. A time step of 1.0 fs was used, and the simulation ran for a total duration of 10 ps [50, 51].

The geometric stability of the TM-doped AsP monolayer was thoroughly assessed using advanced DFT calculations. The specific formula used to accurately calculate the formation energy is given as follows [52]:

$$E_f = E_{AsP-s+TM} - E_{AsP-s} - E_{TM}$$

The $E_{AsP-s+TM}$, E_{TM}, and E_{AsP-s}, denote the energies of the AsP monolayers doped with the TM, the TM atoms and the AsP monolayers, each with one vacant site, respectively.

The optimal adsorption site for a specific gas significantly depends on the type of gas molecules and the corresponding adsorption energy on pristine or TM-doped AsP monolayers. The following formula is used to accurately calculate the adsorption energy for a given system. [53, 54]:

$$E_{ad} = E_{AsP+gas} - E_{AsP} - E_{gas}$$

The $E_{AsP+gas}$, E_{AsP}, and E_{gas}, denote the total energy of the pristine or TM-doped AsP monolayers adsorption system, pristine AsP monolayers or TM-doped AsP monolayers, and the isolated gas molecules, respectively.

In order to gain a much deeper insight into the intricate doping of AsP with five small molecule gases, we employed the following equation to calculate the charge density difference:

$$\Delta\rho = \rho_{total} - \rho_{sub} - \rho_{gas}$$

The ρ_{sub}, ρ_{total} and ρ_{gas} represent the spatial distribution of charge density of TM- doped AsP, TM-doped AsP with adsorbed gas molecules, and gas molecules in the free state, respectively.

The conductivity was calculated using the following equation [55]:

$$\sigma = exp\ （-E_g/2KT）$$

The k and T are the Boltzmann constant (K = 8.62 × 10^{-5} eV/K), the band gap, and the thermodynamic temperature of the configuration, respectively.

The recovery time was calculated using the following equation [56]:

$$\tau = {V_0}^{-1} exp\ （-E_{ads}/KT）$$

The V_0, E_{ads}, K and T are the frequency of light, the adsorption energy, the Boltzmann constant, and the thermodynamic temperature, respectively.

Results and Discussion

Geometric structures of the pristine AsP monolayers, TM-doped AsP monolayers and free molecules

The lattice parameters of the structurally optimized pristine AsP monolayer were determined to be 3.51 Å and 4.65 Å, with an additional folding height of 3.57 Å [57, 58]. As shown in Table S1, the bond lengths for gas molecules CO, NO_2, and NO are measured at 1.144 Å, 1.172 Å, and 1.214 Å, while the bond angle for the non-linear molecule NO_2 is 133.735° [59, 60]. These calculated values align closely with those reported in previous studies, and confirm the accuracy of the computational methods employed. This further substantiates the reliability of the predicted characteristics of the adsorption system.

To determine the most stable configuration of TM-doped AsP monolayers, we thoroughly explored two distinct doping methods: substituting the original arsenic (As) or phosphorus (P) atoms with TM atoms. As shown in Table-1, results indicate that substituting As atoms with TM atoms is more stable than substituting P atoms; thus, we focused primarily on structures where TM atoms replace As atoms. The formation energies for replacing As with gold (Au), silver (Ag), and osmium (Os) are -2.319 eV, -1.252 eV, and -1.954 eV, indicating that this process is exothermic. Among these metals, the Au-AsP monolayer exhibits the lowest energy and highest stability, making it the optimal configuration for further gas adsorption studies. Fig. 4(a) shows that the Au-AsP monolayer did not undergo significant deformation or local structural reconstruction. The bond lengths in the Au-AsP monolayer are very close to those in the undoped model; Specifically, the P1-Au, P2-Au, and As-Au bond lengths are 2.314 Å, 2.313 Å, and 2.512 Å, slightly shorter than the original AsP bond lengths of 2.376 Å and 2.534 Å. In addition, the Au atom is slightly displaced downward by approximately 0.20 Å relative to the original monolayer surface, indicating a minor structural relaxation of the system, which allows for a more energetically favorable configuration without introducing significant lattice distortion.

Stability

Fig. 2(a) shows that the phonon dispersion curve for the AsP monolayer does not exhibit significant imaginary frequencies, indicating stable dynamic properties. To evaluate the feasibility of doping the AsP monolayer for gas sensing applications, we conducted molecular dynamics simulations at room temperature. The molecular dynamics results showed that both pristine and Au-AsP monolayers exhibited minimal total energy fluctuations under these conditions, with no bond breakages observed. This further confirms the high stability of the AsP structure both before and after doping, as illustrated in Fig. 2(b) and 2(c).

Table-1: Relevant parameters for Au, Ag, and Os atomic doping, including formation energy (E_f in eV), work function (WF in eV), transferred electrons (C in e), and Band gap (E_g in eV)

Molecule	Ef(eV)	WF(eV)	C(e)	Eg(eV)
Au_{As}	-2.319	4.744	+0.118	0.240
Au_{P}	-2.315	4.698	+0.191	0.546
Ag_{As}	-1.252	4.686	-0.172	0.002
Ag_{P}	-1.173	4.672	-0.307	0.351
Os_{As}	-1.954	4.760	-0.054	0.131
Os_{P}	-1.308	4.793	-0.173	0.118

Electronic properties of pristine AsP monolayers and TM-doped AsP monolayers

This study calculated the band structures after doping. As shown in Fig. 1(b) and Fig. 6(a), both the pristine AsP monolayer and the Au-doped α-AsP monolayer exhibit a band gap.

To gain a deeper understanding of the fundamental chemical interactions between Au atoms and the pristine AsP monolayer, this study utilizes CDD, PDOS, and charge transfer analyses conducted in a comprehensive manner. The Au-AsP monolayer undergoes notable electronic reorganization. As illustrated in Fig. 5(a), there is evident orbital overlap between the Au:5d, P:3p, and As:4p orbitals, occurring at approximately -8.1 eV, -5.4 eV, and -4.5 eV, respectively. Charge accumulation is primarily observed on the Au atoms, while charge depletion is most pronounced on the As atoms neighboring the Au atoms, as shown in Fig. 4(e). Bader charge analysis reveals that the As atom loses 0.326 electrons, whereas the Au atom gains 0.118 electrons, suggesting that Au atoms act as electron acceptors in this system. The significant electronic transfer from As to Au leads to enhanced local interactions, supporting the covalent nature of the bonding. Additionally, the phosphorus atoms adjacent to Au show different charge behaviors: the upper phosphorus atom gains 0.010 electrons, while the lower phosphorus atom loses 0.060 electrons. This differential charge distribution highlights the remarkably strong and significant chemical interaction between the Au atom and the surrounding atoms. These results further confirm the robust chemical bonding between Au and As atoms, contributing to the system's stability.

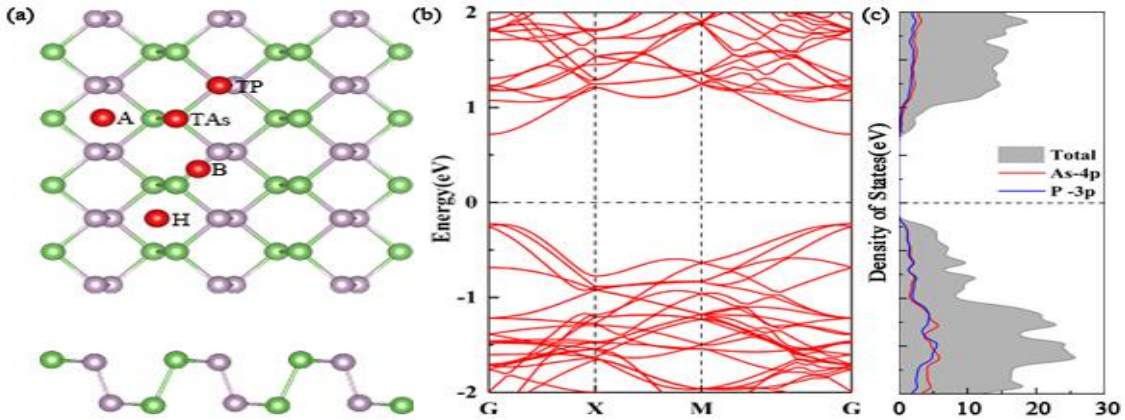

Fig. 1: (a) Top and side views of the geometric structure (purple, green, and red spheres represent phosphorus atoms, arsenic atoms, and the initial adsorption sites of the gas on the pristine AsP structure, respectively), (b) Band structure, (c) Density of States (DOS) for the AsP monolayer. The Fermi energy level is set at zero, marked by a black dashed vertical line.

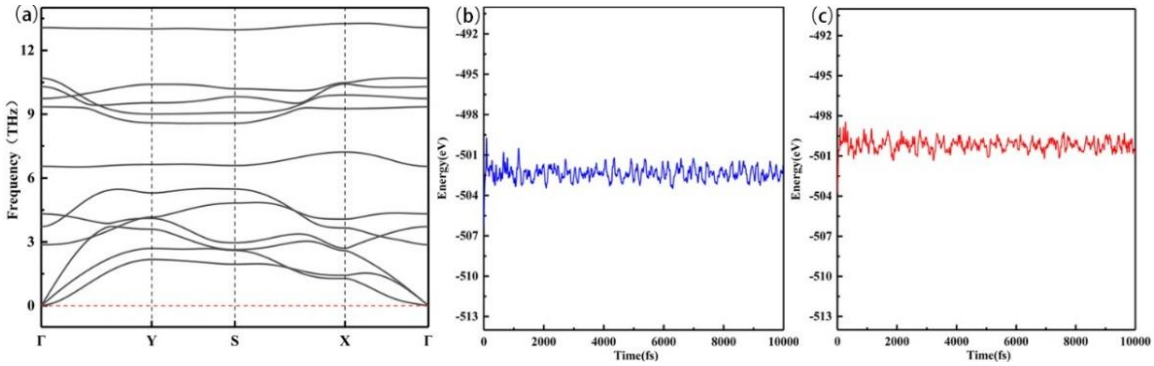

Fig. 2: (a) Phonon dispersion curve of the AsP monolayer; (b) and (c) Energy variation of the pristine and Au-doped AsP monolayers at T = 300 K, respectively.

This study calculates the work function of the AsP monolayer after specific metal atom doping. According to Table 1, the work function of the Au-AsP monolayer is lower than that of the pristine AsP monolayer. A reduced work function facilitates electron emission, which could improve the gas adsorption and sensing capabilities of the AsP monolayer.

Geometric structures of pristine and doped AsP monolayers after gas adsorption

To accurately determine the most stable adsorption configurations of different gas molecules on both pristine and doped AsP monolayers, the gas were initially selectively positioned at various specific locations above the pristine AsP monolayer. As shown in Fig. 1(a), five distinct adsorption sites were considered: atop the As atoms (TAs), atop the P atoms (TP), at the center of the As-P bond (B), and above two different hexagonal centers (H, A). For the Au-AsP monolayer, the gas molecules were positioned directly above the Au atoms.T hree different initial configurations were explored for the gas adsorption on both pristine and doped AsP monolayers. In the first configuration, the diatomic gases CO and NO were placed with the two atoms aligned parallel to the surface of the AsP monolayer. In the second configuration, the bond between the atoms was perpendicular to the surface, further divided into two cases: one where the non-oxygen atoms are closest to the surface, and the other where the oxygen atoms are adjacent. For the nonlinear molecule NO_2, similar parallel and perpendicular orientations were considered. In the perpendicular case, the bond between the two oxygen atoms remained parallel to the surface, with two sub-categories: one where the oxygen atoms are adjacent to the surface and another

where the non-oxygen atoms are closest. All gas molecules are positioned at a distance of 3 Å from the AsP surface.

The pristine AsP monolayer exhibits adsorption energies of less than -0.5 eV for CO, NO_2, and NO gases. Due to these relatively low adsorption energies, the gases are not efficiently adsorbed onto the AsP monolayer, leading to the decision not to pursue further investigation of their adsorption behaviors on this surface.

Subsequently, the study examines the impact of gold (Au) doping on the adsorption performance of the AsP monolayer. The inclusion of Au significantly enhances the material's adsorption capacity for CO, NO_2, and NO. The most stable and favorable adsorption configurations are clearly illustrated in Fig. 4, with detailed parameters for each specific gas molecule before and after adsorption, such as adsorption energy, distance, and charge transfer, provided in Fig. 3.

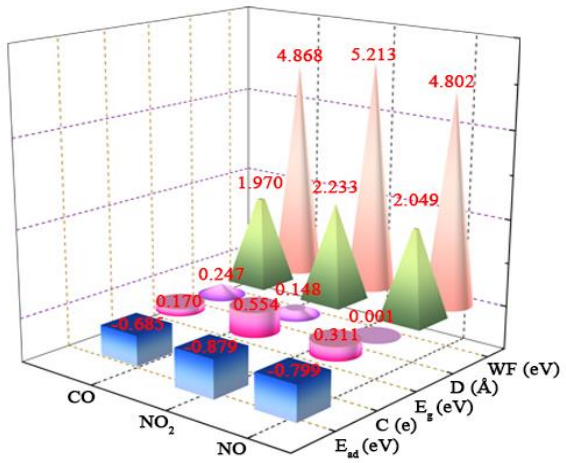

Fig. 3: (a) Data after the adsorption of the corresponding gases. The prismatic shapes represent adsorption energy (E_{ad} in eV), the cylindrical shapes represent electron transfer (C in e), the truncated cones represent the band gap (E_g in eV), the conical frustums represent the adsorption distance (D in Å), and the cones represent the work function (WF in eV). The doped structure forms a compensatory electronic network. These findings highlight the strong chemical interaction between Au and As atoms, further enhancing system stability..

As illustrated in both Fig. 3 and Fig. 4(b),CO adsorption on the Au-AsP monolayer occurs via the carbon atom, with the C–Au distance reducing to 1.970 Å, indicating a clear binding interaction. The adsorption energy of CO is -0.685 eV, demonstrating a stronger adsorption strength on the Au-AsP monolayer compared to the pristine monolayer. In this configuration, the Au-P and Au-As bond lengths increase to 2.395 Å and 2.651 Å. Furthermore, the C–O bond length in CO slightly increases from 1.144 Å to 1.158 Å upon adsorption, suggesting activation and electronic reorganization of the CO molecule. These results confirm a chemical interaction between CO and the Au-AsP monolayer.

As illustrated in both Fig. 3 and Fig. 4(c), NO_2 adsorption on the Au-AsP monolayer occurs via the nitrogen (N) atom, with a C–Au distance of 2.233 Å. The adsorption performance of NO_2 is notably stronger than that of CO and NO, with an adsorption energy of -0.88 eV. Following adsorption, the Au-As, Au-P1, and Au-P2 bond lengths increase to 2.537 Å, 2.522 Å, and 2.525 Å, respectively, indicating a reorganization of the electronic environment around the Au atom and changes in molecular interactions. Additionally, the O–N–O bond angle decreases from 133.735° to 124.769°, signifying a reorientation of the NO_2 molecule during the interaction. The N–O1 and N–O2 bond lengths also increase slightly, from 1.214 Å to 1.233 Å and 1.244 Å, respectively, indicating structural adjustments. These results highlight a significant chemical interaction between the NO_2 and the Au-AsP monolayer, and underscore the enhancing effect of Au on the material's overall adsorption capacity.

As illustrated in both Fig. 3 and Fig. 4(d), NO adsorption on the Au-AsP monolayer occurs through both the nitrogen (N) atom and the Au atom, with a N–Au distance of 2.049 Å. The adsorption strength of NO on the Au-AsP monolayer exceeds that of CO, with an adsorption energy of -0.799 eV. After adsorption, the Au-As, Au-P1, and Au-P2 bond lengths are 2.612 Å, 2.386 Å, and 2.412 Å, respectively. Furthermore, the N–O bond length increases from 1.172 Å to 1.188 Å, indicating slight structural adjustments in the molecule due to adsorption. These results confirm the significant chemical interaction between the NO and the Au-AsP monolayer, and emphasize the crucial role of Au in improving the material's overall adsorption performance.

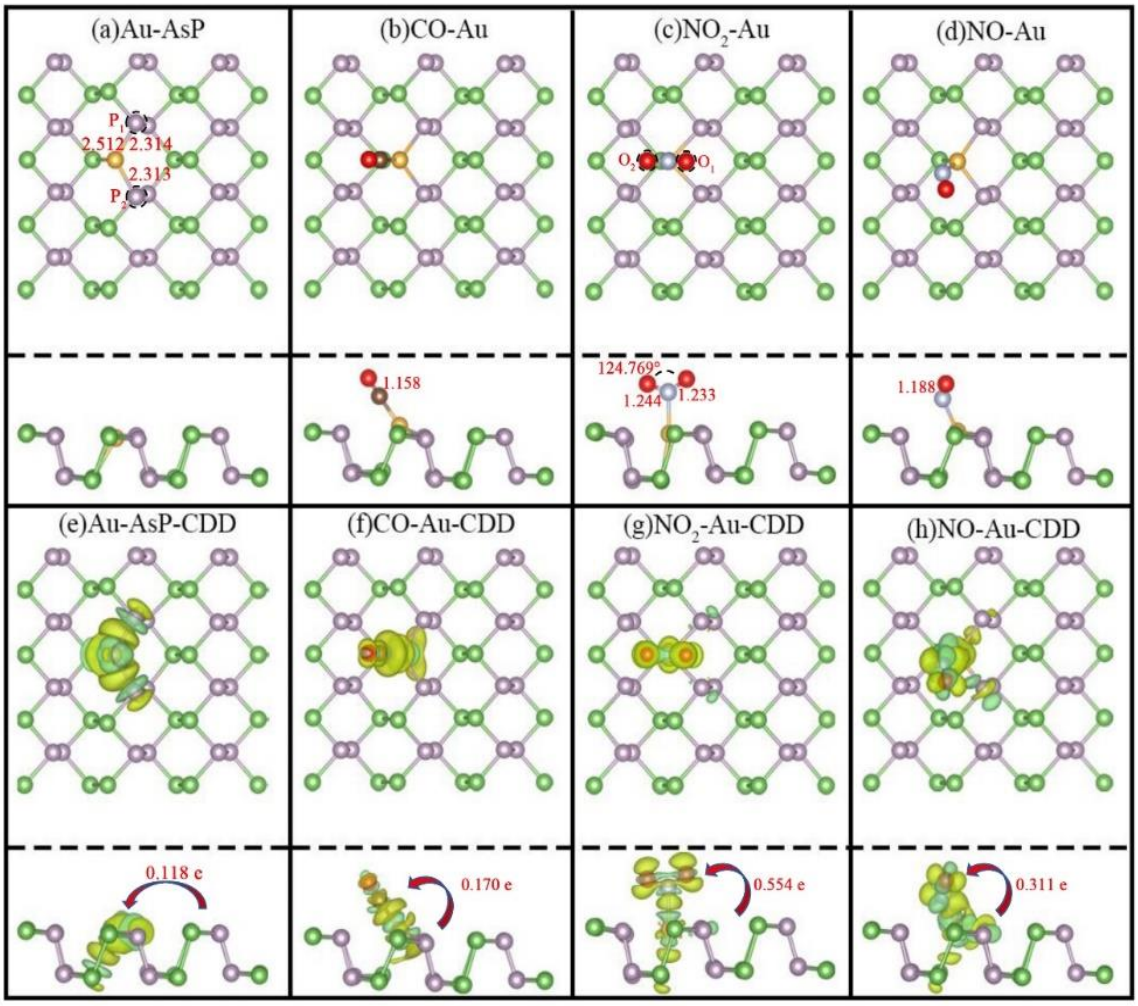

Fig. 4: (a)–(d) and (e)–(h) respectively show the most stable configurations and corresponding charge difference densities of CO, NO_2, and NO adsorbed on the Au-doped AsP surface. Yellow and green represent charge accumulation and depletion, respectively. The isosurface values for CO, NO_2, and NO are set at 0.002 e/Å^3.

Electronic properties of doped AsP monolayers after gas adsorption.

This study calculates PDOS, TDOS, CDD, and charge transfer after adsorption to analyze the system's electronic properties.

The adsorption of CO results in minimal changes to the band structure, indicating a limited effect on the overall electronic structure (Fig. 6(b)). Additionally, the Au:5d orbitals hybridize with the C:2p and O:2p orbitals of CO at energy levels around -9.9 eV, -7.7 eV, -6.9 eV, and -0.1 eV (Fig. 5(b)), suggesting a tendency for chemical bonding between the Au atom and the CO molecule. Bader charge analysis (Fig. 3) shows that the CO molecule gains 0.170 e, while the Au atom loses 0.135 e, indicating the presence of chemisorption. This conclusion is further confirmed by charge density difference analysis, which shows significant electron accumulation around the CO molecule, particularly near the C-Au bond, indicating substantial electron transfer from the gold atom to the CO molecule (Fig. 4(f)). This weak chemical interaction, characterized by notable charge transfer and an adsorption energy exceeding 0.5 eV, enhances CO binding while preserving the integrity of the CO molecule. Such weak chemisorption is beneficial for gas sensing applications, as it stabilizes the CO molecule while preserving effective electronic sensitivity.

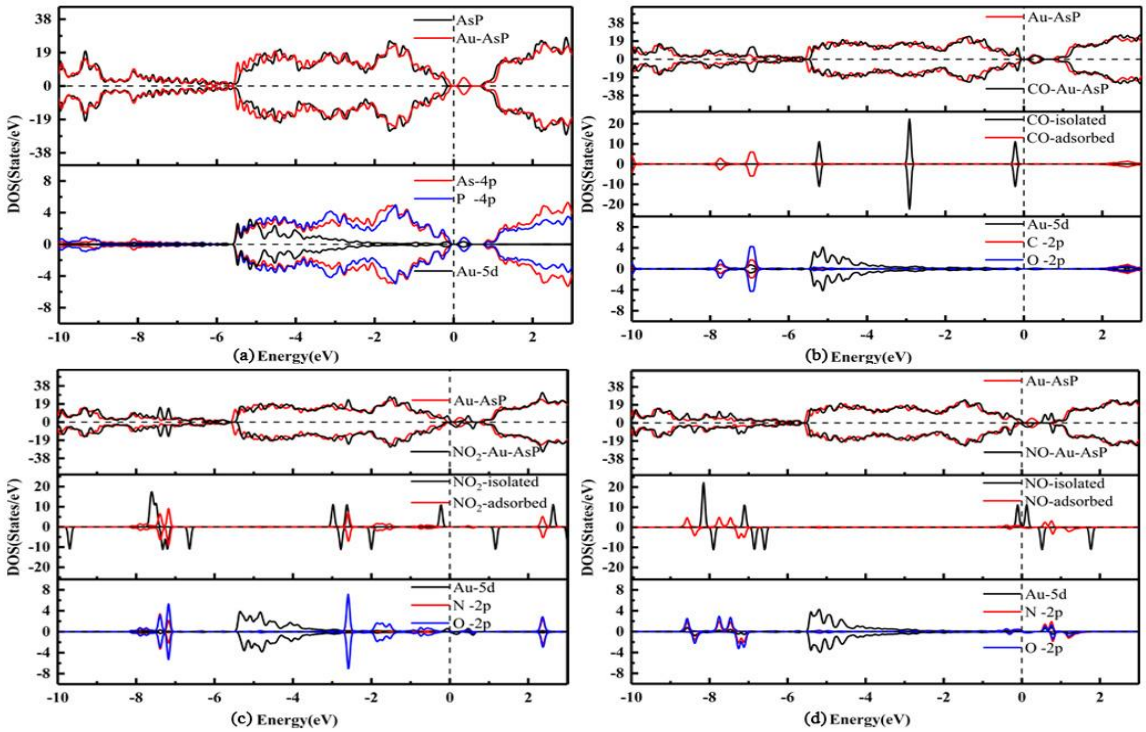

Fig. 5: (a) The DOS of the Au-doped AsP monolayer. The DOS of (b) CO, (c) NO_2, (d) NO gas molecule adsorption on the Au-doped AsP monolayer. The Fermi energy level was positioned at zero as a black dashed vertical line.

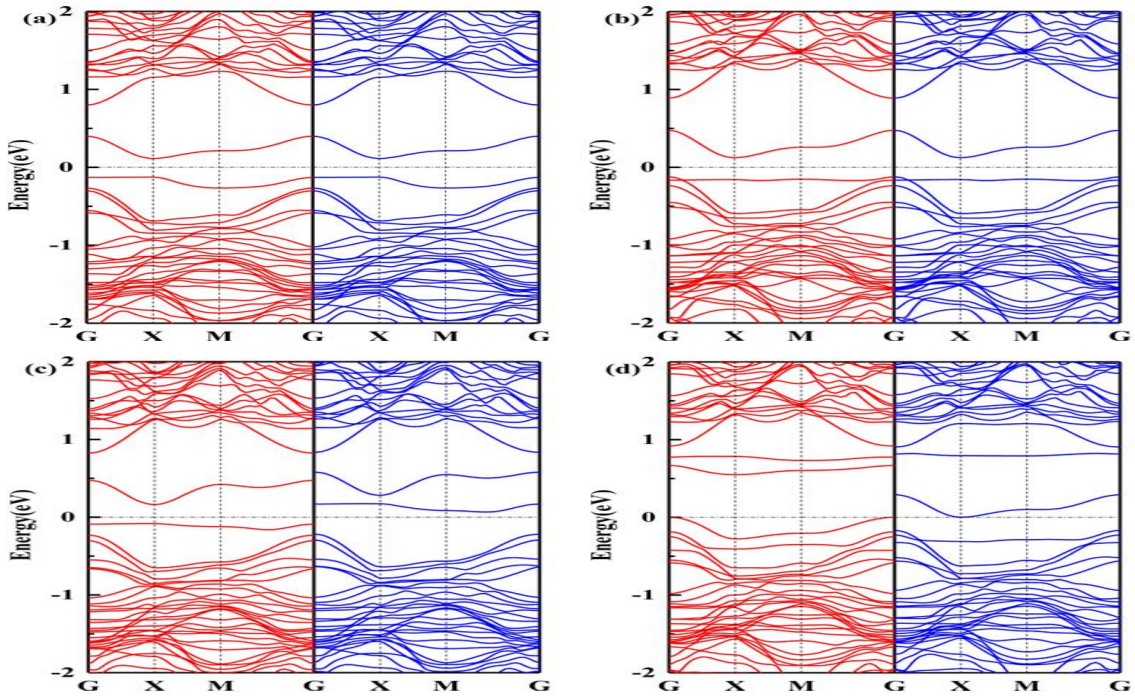

Fig. 6: (a) The band structure of the Au-doped AsP monolayer. The band structures of (b) CO, (c) NO_2, (d) NO gas molecule adsorption on the Au-doped AsP monolayer. The Fermi energy level was positioned at zero as a black dashed vertical line.

The Au-AsP monolayer exhibits notable NO_2 adsorption characteristics, marked by strong electron rearrangement and distinct orbital overlap interactions. As shown in Fig. 6(c), NO_2 adsorption induces spin polarization near the Fermi level, an effect absent before adsorption, indicating a significant alteration in the system's magnetic properties. This provides a potential mechanism for NO_2 detection using Au-AsP monolayer sensors. As shown in Fig. 5(c), orbital overlap between Au:5d, N:2p, and O:2p occurs at energy levels around -8.0 eV, -7.9 eV, -7.7 eV, -7.3 eV, and -7.1 eV, suggesting a tendency for chemical bond formation between Au and NO_2. This hybridization strengthens the interaction between the NO_2 molecule and the AsP surface, demonstrating stable bonding between NO_2 and Au. Bader charge analysis (Fig. 3) shows that the NO_2 molecule gains 0.554 e from the Au-AsP monolayer, while the Au atom also acquires 0.156 e. Meanwhile, two P atoms and one As atom near Au collectively lose 1.156 e, indicating that electron transfer mainly occurs from the substrate to NO_2 and Au. Further analysis of the CDD map provides additional details on the electron transfer. As shown in Fig. 4(g), significant charge accumulation is observed around the oxygen atom of NO_2, with charge depletion near the Au atom, indicating electron transfer from the surrounding substrate regions through Au to the NO_2 molecule. This notable electron accumulation reflects the strong oxidizing nature of NO_2, effectively attracting electrons from the substrate and enhancing its binding with the material surface. These findings indicate that the NO_2 molecule achieves stable chemisorption on the Au-AsP monolayer surface while preserving its molecular integrity.

The Au-AsP monolayer demonstrates notable NO adsorption characteristics, marked by significant electron rearrangement and orbital overlap interactions. As shown in Fig. 6(d), similar to NO_2 adsorption, NO adsorption induces spin polarization, suggesting a change in the system's magnetic characteristics. This provides a potential mechanism for NO detection using an Au-AsP monolayer sensor. As shown in Fig. 5(d), orbital overlap between the Au:5d, N:2p, and O:2p occurs at energy levels around -0.3 eV and from -8.5 to -7.1 eV, suggesting a tendency toward chemical bond formation between Au and NO. This hybridization enhances the interaction between the NO molecule and the AsP surface, indicating stable binding between NO and Au. As shown in Fig. 3, the Bader charge analysis reveals a charge transfer of 0.311 e from the Au-AsP monolayer to the NO molecule, while the Au atom loses 0.233 e. These results align with the charge transfer patterns observed in the CDD map. As illustrated in Fig. 4(h), charge accumulation is prominent near the NO molecule, whereas a depletion is observed around the Au atom, indicating electron transfer from Au to NO. This charge transfer indicates that Au doping can markedly enhance the AsP monolayer's adsorption capacity for NO gas. The findings demonstrate that Au doping enhances the NO sensing capabilities and adsorption of the AsP monolayer, facilitating stable chemisorption.

Potential of doped AsP monolayers structures as gas sensors.

An effective gas sensor should demonstrate favorable response and recovery rates, stability at room temperature, as well as high selectivity and sensitivity [61, 62]. For the Au-AsP monolayer structures examined in this study to be suitable for sensing the three gas molecules under investigation, the adsorption type for these molecules on the doped AsP monolayer should primarily involve chemisorption, characterized by adequate and sufficient charge transfer. This mechanism is essential to prevent spontaneous desorption under ambient conditions and to ensure substantial changes in conductivity.

As shown in Fig. 3, the band gaps of the Au-AsP monolayer upon adsorption of CO, NO_2, and NO gases are 0.247 eV, 0.148 eV, and 0.001 eV. Demonstrate that CO adsorption has minimal impact on the conductivity of the Au-AsP monolayer, suggesting poor sensitivity to CO gas. In contrast, NO_2 adsorption moderately affects conductivity, indicating good sensitivity. In contrast, NO_2 adsorption moderately affects conductivity, indicating good sensitivity. NO adsorption has a significant effect on conductivity, suggesting high sensitivity for NO gas. Since gas sensors detect molecules by measuring changes in conductivity following adsorption, this study calculated the conductivity at T=300 K after adsorption, as shown in Table 2. Results show that although the change in band gap due to CO gas adsorption is minimal, the conductivity changes by more than 10%. Therefore, judging by the conductivity, the Au-AsP monolayer exhibits an appropriate conductivity change and certain sensitivity to CO gas adsorption.

Table-2: Relevant parameters for the adsorption of CO, NO_2, and NO gas molecules on the Au-doped AsP surface, including bond length (Å), bond angle (°), electrical conductivity (σ).

Molecule	Bond length (Å)	Angle (°)	σ
CO	1.15 (C-O)	/	8.43×10^{-3}
NO_2	1.23(N-O_1)	124.7°	5.71×10^{-2}
	1.24(N-O_2)		
NO	1.18 (N-O)	/	9.80×10^{-2}

To comprehensively evaluate the potential of Au-doped monolayer AsP in gas sensing applications, this study quantitatively analyzed the system's work function variations upon adsorption of various small gas molecules. As shown in Fig. 3, due to its electron-accepting properties, NO_2 gas gained 0.554 e of charge during adsorption, resulting in an increase in the system's work function from 4.744 eV to 5.213 eV. Similarly, NO and CO gases received 0.311 e and 0.170 e of charge upon adsorption, leading to increases in the system's work function to 4.802 eV and 4.868 eV. The notable increase in work function shows that all three gases, especially NO_2, exhibit good selectivity when detected by the Au-AsP sensor.

This study calculated the recovery times for the adsorption systems under conditions of $V_0 = 10^{14}$ s^{-1} and T = 300 K. As shown in Table 2, the doping of Au in the AsP monolayer results in a desorption time of 0.262 s for NO gas. For NO_2 gas, the desorption time is 5.78 s under the same conditions, and similarly, the desorption time for CO gas is 0.003 s.

As shown in Table 3, when the dopant atoms are all Au, the Au-AsP monolayer studied in this work exhibits extremely short response and recovery times for CO gas detection, whereas compared with the Au-doped $SnSe_2$ monolayer, which shows a 4-second response and recovery time for CO gas, the Au-AsP monolayer demonstrates even shorter times. This indicates that the Au-AsP monolayer investigated in this study significantly outperforms the aforementioned materials in terms of response speed and recovery capability for CO gas sensing, highlighting its substantial application potential.

Table-3: Doped with Au atoms. Recovery(response) time (τ in s) of the gas molecules after adsorption at T = 300 K.

Molecule	τ（s）	Source
CO	3.19×10^{-3}	This work
NO2	5.78	
NO	2.62×10^{-1}	
CO	4	[41]
NO	7	
NO2	11	[42]

In terms of NO gas detection, the response and recovery times of the Au-AsP monolayer, which are less than 1 second, are longer than those of another AsP monolayer, but still significantly shorter than those of the Au-doped $SnSe_2$ monolayer. Furthermore, the adsorption of NO gas has a pronounced effect on the electrical conductivity of the Au-AsP monolayer, further enhancing its sensing performance. Therefore, the Au-AsP monolayer not only exhibits high sensitivity and good selectivity for NO gas detection, but also features rapid response and recovery characteristics, making it a promising candidate for NO gas sensing applications.

For NO_2 gas, although the response and recovery times of the Au-AsP monolayer are longer compared to those for CO and NO, they are still markedly superior to those of the other AsP monolayer and remain within an acceptable range. At the same time, the adsorption of NO_2 induces a moderate change in the electrical conductivity of the Au-AsP monolayer, providing a reasonable sensitivity. Combined with its good selectivity and relatively short response time, the Au-AsP monolayer also demonstrates strong capability in NO_2 detection.

In summary, the Au-AsP monolayer proposed in this study demonstrates excellent sensing performance for CO, NO, and NO_2 gases. In particular, for CO and NO_2 gases, it significantly outperforms the alternative AsP monolayer structure and the Au-doped $SnSe_2$ monolayer in terms of response speed and recovery capability. While the response and recovery times for NO gas are slightly longer compared to the alternative AsP monolayer structure, they are still under 1 second, proving its excellent response speed and recovery capability. This highlights its broad application prospects as a versatile gas sensing material.

Conclusion

This study assesses the stability of pristine AsP monolayers through molecular dynamics simulations and phonon dispersion analysis. Additionally, molecular dynamics simulations confirm the dynamic stability of Au-AsP monolayers. The investigate the nature of gas adsorption and the strength of molecular interactions by examining the geometric structure, adsorption energy, electron density, electron transfer, and DOS of Au-AsP monolayers before and after the adsorption of CO, NO, and NO_2. Additionally, the conductivity and recovery time following gas adsorption are calculated from

energy band structures and adsorption energies to assess the potential of Au-AsP monolayers as sensors for these gases. Finally, through the work function and conductivity analyses, the results demonstrate that Au-AsP monolayers are highly sensitive sensors for NO and NO_2 gases, as well as efficient sensors for high concentrations of CO. This study aims to propose that Au doping can modulate the interactions between gas and the most stable α-phase AsP monolayer, providing new insights into using the Au-doped α-phase AsP monolayer for detecting specific toxic gases.

Acknowledgments

Thanks to the high-performance computing platform of Henan Polytechnic University for the assistance provided.

References

1. R. Sardaro,G. De Pascale,C. Ingrao,N. Faccilongo. Latent relationships between environmental impacts of cultivation practices and land market: evidences from a spatial quantile regression analysis in Italy, *Journal of Cleaner Production*, **279**, 123648 (2021).
2. C. He, X. Zhao, M. Huo *et al*. Surface, interface and structure optimization of metal-organic frameworks: towards efficient resourceful conversion of industrial waste gases, The *Chemical Record*, **23**, e202200211 (2023).
3. T. Yang,W. Liu. Health effects of energy intensive sectors and the potential health Co-benefits of a low carbon industrial transition in china, International *Journal of Environmental Research and Public Health*, **16**, 3022 (2019).
4. Z. Li,M. Liu,C. Fang *et al*. Aluminium-based MOF CAU-1 facilitates effective removal of florfenicol via hydrogen bonding, *J Saudi Chem Soc*, **28**, 101879 (2024).
5. E. Anyanwu. Complex interconvertibility of nitrogen oxides (NOX): impact on occupational and environmental health, *Rev Environ Health*, **14**, 169 (1999).
6. D. O. Johns,W. S. Linn. A review of controlled human SO_2 exposure studies contributing to the US EPA integrated science assessment for sulfur oxides, *Inhal Toxicol,* **23**, 33 (2011).
7. X. Jia,L. An. The adsorption of nitrogen oxides on noble metal-doped graphene: the first-principles study, *Mod Phys Lett B*, **33**, 1950044 (2019).
8. E. Salih,A. I. Ayesh. Enhancing the sensing performance of zigzag graphene nanoribbon to detect NO, NO_2, and NH_3 gases, *Sensors*, **20**, E3932 (2020).
9. W. Zhang, Y. Yong, Z. Li *et al*. First-principles study of highly sensitive and selective gas-sensing properties of the C_3N_2 monolayers towards SO_2 gas, *Surf Interfaces*, 33, 102254 (2022).
10. A. Abbasi. Adsorption of phenol, hydrazine and thiophene on stanene monolayers: A computational investigation, *Synth Met*, **247**, 26 (2019).
11. A. Abbasi. Modulation of the electronic properties of pristine and AIP-codoped stanene monolayers by the adsorption of CH2O and CH4 molecules: a DFT study, *Mater Res Express*, **6**, (2019).
12. A. Abbasi,R. M. Rzayev,A. A. Niyazova *et al*. Enhanced adsorption and biosensing performance of adenine (C5H5N5) and guanine (C5H5N5O) nucleobases on the novel ZnO-MoSe2 nanosheets: A theoretical study, *Mater Chem Phys*, **337**, (2025).
13. A. Abbasi,J. J. Sardroodi. Adsorption of O3, SO2 and SO3 gas molecules on MoS2 monolayers: A computational investigation, *Appl Surf Sci*, **469**, 781 (2019).
14. A. Abbasi, A. Abdelrasoul, J. J. Sardroodi. Adsorption of CO and NO molecules on Al, P and Si embedded MoS2 nanosheets investigated by DFT calculations, *Adsorpt J Int Adsorpt Soc*, **25**, 1001 (2019).
15. A. Abbasi, J. J. Sardroodi. Exploration of sensing of nitrogen dioxide and ozone molecules using novel TiO2/Stanene heterostructures employing DFT calculations, *Appl Surf Sci*, **442**, 368 (2018).
16. A. Abbasi,J. J. Sardroodi. The adsorption of sulfur trioxide and ozone molecules on stanene nanosheets investigated by DFT: Applications to gas sensor devices, *Physica E*, **108**, 382 (2019).
17. A. Abbasi,J. J. Sardroodi. An innovative gas sensor system designed from a sensitive nanostructured ZnO for the selective detection of SOx molecules: a density functional theory study, *New J Chem*, **41**, 12569 (2017).
18. A. Abbasi, J. J. Sardroodi. A highly sensitive chemical gas detecting device based on N-doped ZnO as a modified nanostructure media: A DFT plus NBO analysis, *Surf Sci*, **668**, 150 (2018).
19. C. Qin, Y. Wang, Y. Gong, Z. Zhang, J. Cao. CuO-ZnO hetero-junctions decorated graphitic carbon nitride hybrid nanocomposite: Hydrothermal synthesis and ethanol gas sensing application, *J Alloys Compd*, **770**, 972 (2019).
20. W. Wei,X. Qu. Extraordinary physical properties of functionalized graphene, *Small*, **8**, 2138 (2012).
21. A. Abbasi. Tuning the structural and electronic properties and chemical activities of stanene monolayers by embedding 4d Pd: a DFT study, *RSC Adv*, **9**, 16069 (2019).

22. A. Abbasi,J. J. Sardroodi. Density functional theory investigation of the interactions between the buckled stanene nanosheet and XO2 gases (X = N, S, C), *Comput Theor Chem*, **1125**, 15 (2018).
23. W. Yuan,L. Huang,Q. Zhou,G. Shi. Ultrasensitive and selective nitrogen dioxide sensor based on self-assembled graphene/polymer composite nanofibers, *ACS Appl Mater Interfaces*, **6**, 17003 (2014).
24. L. Yangfan,W. Tianxing,A. Yipeng,D. Xiao. Properties of B- and Si-doped monolayer black phosphorus under biaxial strain, *Results Phys*, **54**, 107091 (2023).
25. T. Ma,H. Huang,W. Guo *et al*. Recent progress in black phosphorus sensors, *J Biomed Nanotechnol,* **16**, 1045 (2020).
26. J. Song, L. Chai,Y. Liang *et al*. Direct gas phase synthesis of high-purity black arsenic phosphorus with non-metallic mineralizer, *J Alloys Compd*, 956, 170256 (2023).
27. R. Han,S. Feng,D.-M. Sun,H.-M. Cheng. Properties and photodetector applications of two-dimensional black arsenic phosphorus and black phosphorus, *Sci China Inf Sci*, **64**, (2021).
28. M. Xie,S. Zhang,B. Cai *et al*. A promising two-dimensional solar cell donor: black arsenic-phosphorus monolayer with 1.54 eV direct bandgap and mobility exceeding 14,000 $cm^2 V^{-1} s^{-1}$, *Nano Energy*, **28**, 433 (2016).
29. B. Liu,M. Koepf,A. N. Abbas *et al*. Black arsenic-phosphorus: Layered anisotropic infrared semiconductors with highly tunable compositions and properties, *Adv Mater*, **27**, 4423 (2015).
30. F. Liu, X. Zhang, P. Gong *et al*. Potential outstanding physical properties of novel black arsenic phosphorus $As_{0.25}P_{0.75}/As_{0.75}P_{0.25}$ phases: a first-principles investigation, *RSC Adv,* **12**, 3745 (2022).
31. L. Yu,Z. Zhu,A. Gao *et al*. Electrically tunable optical properties of few-layer black arsenic phosphorus, *Nanotechnology*, **29**, 484001 (2018).
32. J. Wang,G. Yang,J. Xue *et al*. High sensitivity and selectivity of AsP sensor in detecting SF6 decomposition gases, *Sci Rep*, **8**, 12011 (2018).
33. T. Wang,X. Li,L. Li,D. Li. First-principles study of gas adsorption and sensing based on noble metal (Ag, Au and Pt)- decorated α-AsP monolayer*, J Mol Graph Modell*, **116**, 108236 (2022).
34. F. Shojaei,H. S. Kang. Electronic structure and carrier mobility of two-dimensional α arsenic phosphide, *J Phys Chem C*, **119**, 20210 (2015).
35. L. Lin,Z. Feng,Z. Dong *et al*. Adsorption of small gas molecules of transition metal (Pt and Au) modified $HfSe_2$ monolayer, Mater Today *Commun*, **32**, 103885 (2022).
36. K. Ding,Y. Lin,M. Huang. The enhancement of NO detection by doping strategies on monolayer MoS_2, *Vacuum*, **130**, 146 (2016).
37. K. Wang,J. Pang,G. Wei,Y. Zhong,S. Wei. C-doped CdS_2 monolayer as toxic gas scavenger or sensor based on first-principles study, *Chem Phys Lett*, **855**, 141570 (2024).
38. D. Ma,W. Ju,T. Li *et al*. The adsorption of CO and NO on the MoS_2 monolayer doped with Au, Pt, Pd, or Ni: A first-principles study, *Appl Surf Sci*, **383**, 98 (2016).
39. D. Li,X. Li,T. Wang,L. Li,J. Wang. H2S gas sensitivity of doped SbP monolayer:first principle study, *J Chem Soc Pak,* **45**, 173 (2023).
40. J. Prasongkit,V. Shukla,A. Grigoriev,R. Ahuja,V. Amornkitbamrung. Ultrahigh-sensitive gas sensors based on doped phosphorene: a first-principles investigation, *Appl Surf Sci*, 497, 143660 (2019).
41. L. Lin,D. Pang,P. Shi *et al*. Strain facilitated small gas molecules sensing properties on Au doped $SnSe_2$ monolayer, *Int J Hydrog Energy*, **47**, 14361 (2022).
42. T. Wang,X. Li,J. Wang,L. Li,D. Li. Two-dimension black arsenic-phosphorus as a promising NO sensor: a DFT study, *Comput Theor Chem*, **1213**, 113727 (2022).
43. Kresse,Furthmuller. Efficient iterative schemes for ab initio total-energy calculations using a plane-wave basis set, Phys Rev B: *Condens Matter Mater Phys*, **54**, 11169 (1996).
44. C. Lu,W. Gong,Q. Li,C. Chen. Elucidating stress-strain relations of ZrB_{12} from first-principles studies, *J Phys Chem Lett*, **11**, 9165 (2020).
45. Perdew, Burke, Ernzerhof. Generalized gradient approximation made simple, *Phys Rev Lett*, **77**, 3865 (1996).
46. L. Simon, J. M. Goodman. How reliable are DFT transition structures? Comparison of GGA, hybrid-meta-GGA and meta-GGA functionals, *Org Biomol Chem*, **9**, 689 (2011).
47. J. Witte, N. Mardirossian, J. B. Neaton, M. Head-Gordon. Assessing DFT-D3 damping functions across widely used density functionals: Can we do better?, *Journal of Chemical Theory and Computation*, **13**, 2043 (2017).
48. D. Chen, X. Zhang, J. Tang *et al*. Adsorption and dissociation mechanism of SO_2 and H_2S on Pt decorated graphene: a DFT-D3 study, *Applied Physics A-Materials Science & Processing,* **124**, 404 (2018).
49. K. Wang, J. Pang, G. Wei, Y. Zhong, S. Wei. First-principles study on CdS_2 monolayer as toxic gas sensor or scavenger, *Chem Select*, 9, e202304840 (2024).
50. Hoover. Canonical dynamics: equilibrium phase-

space distributions, *Phys Rev A*, **31**, 1695 (1985).
51. S. Nosé. A unified formulation of the constant temperature molecular dynamics methods., *J Chem Phys*, **81**, 511 (1984).
52. L. Han,L. Lin, K. Xie *et al*. Adsorption and sensing of CO on VS_2 monolayer decorated with transition metals (Cr, Mn, Fe, Co, Ni): a first-principles study, *FlatChem*, **34**, 100389 (2022).
53. O. Leenaerts,B. Partoens,F. M. Peeters. Adsorption of H_2O, NH_3, CO, NO_2, and NO on graphene: a first-principles study, *Phys Rev* B, 77, 125416 (2008).
54. B. Zhang, Z. Wang, H. Huang *et al*. Work function and band alignment of few-layer violet phosphorene, *Journal of Materials Chemistry* A, 8, 8586 (2020).
55. F. Opoku,P. P. Govender. Adsorption behaviour of Si anchored on g-C_3N_4/graphene van der waals heterostructure for selective sensing of toxic gases: insights from a first-principles study, *Appl Surf Sci*, **525**, 146590 (2020).
56. Y. Shen,H. Liu,Q. Zhang *et al*. First principles study on toxic gas adsorption of $PtSe_2$/GaN heterostructure modified by Cu-group elements, *Appl Surf Sci*, **670**, 160678 (2024).
57. B. Karki, M. Rajapakse, G. U. Sumanasekera, J. B. Jasinski. Structural and thermoelectric properties of black arsenic-phosphorus, *Acs Appl Energ Mater*, **3**, 8543 (2020).
58. Y. Sun, Z. Shuai, D. Wang. Lattice thermal conductivity of monolayer AsP from first-principles molecular dynamics, *Phys Chem Chem Phys*, **20**, 14024 (2018).
59. L. Lin, L. Han, K. Xie, C. Hu, Z. Dong. First-principles study of (Ni, Pd, Au)-embedded VS_2 monolayers for adsorption of CO, H_2S, NO, NO_2 and SO_2, *FlatChem*, **36**, 100421 (2022).
60. Y. Zou,F. Li,Z. H. Zhu *et al*. An ab initio study on gas sensing properties of graphene and Si-doped graphene, *Eur Phys J* B, **81**, 475 (2011).
61. A. Aasi,S. M. Aghaei,B. Panchapakesan. Outstanding performance of transition-metal-decorated single-layer graphene-like BC_6N nanosheets for disease biomarker detection in human breath, *ACS Omega*, **6**, 4696 (2021).
62. J. Z. Ou,W. Ge,B. Carey *et al*. Physisorption-based charge transfer in two-dimensional SnS_2 for selective and reversible NO_2 gas sensing, *ACS Nano*, **9**, 10313 (2015).